SSC18-VIII-03

Improved Model for Low Cost Sun Sensor Attitude Filtering

Nicholas J. DiGregorio
University at Buffalo Nanosatellite Laboratory
333 Hochstetter Hall, University at Buffalo, Buffalo NY, 14260
njdigreg@buffalo.edu

Faculty Advisor: Dr. John Crassidis
University at Buffalo, State University of New York

ABSTRACT

A new Sun sensor measurement model is designed and implemented in the attitude estimation system of a simulated spacecraft in low-Earth orbit (LEO) subject to environmental disturbance torques. This new measurement model remains compatible with all previous iterations of coarse Sun sensor hardware, it is merely the data processing that is different. Two Unscented Kalman Filters (UKF) are run in parallel onboard the simulated satellite – one filter using a standard Sun sensor measurement model and the other using the new measurement model. All other details and inputs to the two filters are identical. The results of the two attitude filters are compared to evaluate the performance of the new measurement model and the source of improvement is discussed.

INTRODUCTION

Motivation

Attitude determination and control (ADC) is a critical component of any spacecraft mission. As small satellite missions continue to grow in complexity, the requirements imposed on spacecraft subsystems grow more stringent as well. Unfortunately, budgets available to meet these more complex mission requirements are averse to such growth. This establishes the need for engineers of small spacecraft to be able to do less with more, particularly on subsystems such as ADC, where components can easily reach prices in the tens of thousands of dollars.

Sun sensor systems are an example of one such component that can be extraordinarily expensive. However, while very expensive fine Sun sensor systems are available, coarse Sun sensor systems may be constructed from an array of simple photodiodes that can cost under one dollar each. This potential cost-saving is advantageous to organizations building small satellites, but systems based on coarse sun sensors experience reduced performance compared to the fine sun sensor systems.

In order to meet the challenges imposed by ever-growing mission ambition, a new coarse Sun sensor measurement model is designed and implemented. The new proposed measurement model, hereafter referred to as the voltage measurement model (VMM), allows for more accurate and robust attitude estimation with simple and inexpensive hardware.

This work first presents the standard model currently used for Sun sensor systems in attitude estimation, hereafter referred to as the Sun measurement model (SMM), and then introduces the VMM. The two models are directly compared using simulation, described in the next section. The rotational equations of motion are described, and then the modeling of external environmental disturbance torques is explained. The method by which sensor readings are simulated based on the true dynamic state is then presented. Finally, the simulation results are presented and discussed. The simulation is run with two Unscented Kalman filters (UKF) in parallel. The first filter utilizes the VMM, while the second uses the standard SMM. Since both filters are run in parallel, they are subject to identical external disturbances and an identical sensor array. Thus, difference in performance is due entirely to the proposed new measurement model.

Sun Sensor Standard Measurement Model

Coarse Sun sensors are typically composed of photodiodes, electrical components that have an output voltage proportional to incident light intensity. Photodiodes may also be considered to have electrical current as an output, as it is straightforward to convert between the two. The output voltage will be a fraction of the maximum calibrated output, as given by [1]

$$V_j = \begin{Bmatrix} V_{max}(\boldsymbol{n_j} \cdot \boldsymbol{s}) & \text{for } \boldsymbol{n_j} \cdot \boldsymbol{s} > 0 \\ 0 & \text{for } \boldsymbol{n_j} \cdot \boldsymbol{s} \leq 0 \end{Bmatrix}, \quad (1)$$

where V_j is the voltage across photodiode j, V_{max} is the calibrated maximum voltage, $\boldsymbol{n}_j$ is the outward normal of the photodiode, and $\boldsymbol{s}$ is the vector to the Sun. An algorithm to predict the vector to the Sun, $\boldsymbol{s}_{predict}$, from the date is provided as Algorithm 29 in Vallado [2]. Details of photodiode calibration can be read about in Springmann [3]. The vector to the Sun and the outward normal of the photodiodes may be expressed in any reference frame, as long as they are both in the same reference frame.

Markley and Crassidis [1] provide a method to directly calculate the Sun vector, $\boldsymbol{s}$, when six photodiodes are used. However, to build redundancy into a design, it is often desirable to include more than six photodiodes. When this is done, the system becomes overdetermined and must be solved by the linear least squares problem

$$\boldsymbol{s} = (N^T N)^{-1} N^T \left(\frac{V_j}{V_{max}}\right), \quad (2)$$

where N is a matrix containing the transpose of the outward normal of each photodiode, $\boldsymbol{n}_j^T$. The computed Sun vector $\boldsymbol{s}$ is then compared to $\boldsymbol{s}_{predict}$ inside the UKF in the attitude estimation process. This SMM formulation allows an arbitrary number of photodiodes to be used in the Sun sensor system, increasing both the accuracy and robustness of attitude estimation relative to restricting the number of photodiodes to six..

Matters are complicated, however, by the fact that photodiodes start to deviate from the behavior modeled by equation (1) when the angle of incidence becomes large, typically more than 60°. This is due to internal reflection within the photodiode imposing extra noise upon the reading, as well as the possibility of specular reflection off of other spacecraft surfaces. Rather than attempting to model these error sources that occur at large incidence angles, it is often preferred to simply throw out a voltage reading that is too low. This is because including an additional reading based on a faulty error model is unlikely to produce better performance than simply neglecting that same reading would. However, if too many readings are thrown out, then the overdetermined system can become underdetermined, making it impossible to compute a three-dimensional vector to the Sun. This is where the utility of the newly proposed voltage measurement model comes in.

Voltage Measurement Model

The basis of the newly designed VMM is to avoid the possibility of posing an underdetermined problem. Rather than the UKF comparing predictions and measurements of the Sun vector, predictions and measurements of the photodiode voltages are passed in directly. These voltage measurements take the place of vector measurements. There are two advantages to this approach. The first is that a vector no longer needs to be computed, so the possibility of an underdetermined system is eliminated. This means that even if only one or two photodiodes are producing valid readings, the sun sensor system may still contribute to attitude estimation instead of being left out entirely. The second is that with the SMM, regardless of how many photodiodes are used to compute the Sun vector, it still results in only a single vector measurement for the attitude filter to process. A Sun vector measurement computed from three photodiodes is given the same weight by the filter as a Sun vector measurement computed from 20 photodiodes, despite the latter situation providing more information.

The predicted voltages for the VMM can be calculated similarly to equation (1), except the predicted Sun vector [2] and the present attitude estimate are required. The predicted voltage across the jth photodiode is

$$V_{j,predict} = \begin{Bmatrix} V_{max}(\boldsymbol{n_j} \cdot \boldsymbol{s_{body}}) & \text{for } \boldsymbol{n_j} \cdot \boldsymbol{s_{body}} > 0 \\ 0 & \text{for } \boldsymbol{n_j} \cdot \boldsymbol{s_{body}} \leq 0 \end{Bmatrix} \quad (3)$$

$$\boldsymbol{s}_{body} = A_{est} \boldsymbol{s}_{predict} \quad (4)$$

where $\boldsymbol{s}_{body}$ is the predicted Sun vector rotated into the spacecraft body reference frame by the attitude matrix A_{est}, and $\boldsymbol{s}_{predict}$ is the predicted Sun vector expressed in Earth-Centered Inertial (ECI) coordinates. The attitude matrix that rotates vectors from the ECI frame to the spacecraft body frame can be computed by transforming the quaternion output from the UKF into a rotation matrix. Using the Shuster convention for quaternions, in which the first three components are a complex vector and the fourth component is a real scalar, this operation is given as [1]

$$A(\boldsymbol{q}) = ({q_4}^2 - \|\boldsymbol{q_{1:3}}\|^2) I_3 - 2q_4[\boldsymbol{q_{1:3}} \times] + 2\boldsymbol{q_{1:3}}\boldsymbol{q_{1:3}}^T \quad (5)$$

where A is the attitude matrix computed from quaternion $\boldsymbol{q}$, I_3 is a 3x3 identity matrix and $[\boldsymbol{q_{1:3}}\times]$ indicates the cross product matrix, given by

$$[\boldsymbol{q_{1:3}} \times] = \begin{bmatrix} 0 & -q_3 & q_2 \\ q_3 & 0 & -q_1 \\ -q_2 & q_1 & 0 \end{bmatrix}. \quad (6)$$

With this new proposed voltage measurement model, the voltage V_j measured by photodiode j and the predicted voltage across that photodiode, $V_{j,predict}$, are passed into an attitude filter together with the standard deviation of electrical noise associated with the photodiode hardware, σ_{ss}. This value may be obtained either from a hardware

datasheet or determined experimentally, and is used in weighting the filter measurement covariance, *R*.

Next, the numerical methodology used in testing the new measurement model performance is explained.

NUMERICAL METHODOLOGY

Equations of Motion

The equations of motion of a satellite may be broken into two independent components: translational and rotational. The translational motion is described by orbital mechanics, while the rotational motion is described by attitude dynamics. For the present work, the simple two-body problem as described by Vallado [2] and Bate, Mueller, and White [4] is an adequate representation of the orbital motion.

The angular rate dynamics of a satellite in orbit are given by Euler's rotational equations [5],

$$J\dot{\boldsymbol{\omega}} = -\boldsymbol{\omega} \times J\boldsymbol{\omega} - \boldsymbol{\omega} \times J_w(\boldsymbol{\omega} + \boldsymbol{\Omega}) - J\dot{\boldsymbol{\Omega}} + \boldsymbol{L}\,, \tag{7}$$

where J is the moment of inertia of the satellite, $\boldsymbol{\omega}$ is the angular velocity of the spacecraft, J_w is the moment of inertia of reaction wheels, $\boldsymbol{\Omega}$ is the angular velocity of reaction wheels, and $\boldsymbol{L}$ is the external disturbance torque. None of the simulations in the present work include reaction wheels or control torques, so the previous equation reduces to

$$\dot{\boldsymbol{\omega}} = J^{-1}(-\boldsymbol{\omega} \times J\boldsymbol{\omega} + \boldsymbol{L}\,). \tag{8}$$

After calculating the angular velocity of the spacecraft, the closed form quaternion update equation [1] is used to propagate the attitude quaternion, $\boldsymbol{q}$, from the previous time step to the current one,

$$\boldsymbol{q}_{new} = \left(I_4 + \frac{\Delta t}{2}\begin{bmatrix} -[\boldsymbol{\omega}\times] & \boldsymbol{\omega} \\ -\boldsymbol{\omega}^T & 0 \end{bmatrix}\right)\boldsymbol{q}, \tag{9}$$

where $\boldsymbol{q}_{new}$ is the attitude quaternion at the current time step, I_4 is a 4x4 identity matrix, Δt is the time step, and $[\boldsymbol{\omega}\times]$ indicates the cross product matrix, given by

$$[\boldsymbol{\omega}\times] = \begin{bmatrix} 0 & -\omega_3 & \omega_2 \\ \omega_3 & 0 & -\omega_1 \\ -\omega_2 & \omega_1 & 0 \end{bmatrix}. \tag{10}$$

The rigid body dynamics of equation (8) relates torques to the change in angular velocity, and the attitude kinematics of equation (9) relate the angular velocity to changes in attitude. Together, they fully specify the rotational orientation of a spacecraft in three dimensions. All that is needed is a method to compute the disturbance torques $\boldsymbol{L}$ within equation (8).

Disturbance Torques

Spacecraft in orbit around Earth are subject to disturbance torques from the environment. These disturbances include aerodynamic drag, the residual magnetic dipole, solar radiation pressure, and gravity gradient. These disturbances may not be predicted *a priori* due to their pseudo-random nature, but their approximate magnitude may be computed and their effect on the system modeled using a Gaussian distribution.

The aerodynamic disturbance torque arises from the thin layer of the atmosphere still present in LEO imposing drag on the spacecraft. This torque, $\boldsymbol{L}_{Aero,}$ is calculated using the standard equation for drag and the vector between the center of aerodynamic pressure, $\boldsymbol{r}_{cp}$ and the center of mass, $\boldsymbol{r}_{cm}$ [6], as

$$\boldsymbol{L}_{Aero} = \frac{1}{2}\rho C_d A V^2(\boldsymbol{r_{cp}} - \boldsymbol{r_{cm}}), \tag{11}$$

where ρ is the atmospheric density, C_d is the drag coefficient, A is the reference surface area, and V is the orbital velocity. The density is obtained from an atmospheric model [7], and the drag coefficient is conservatively assumed to be *2.5* [6]. The velocity comes from the orbit propagator in the simulation, and the area and vectors come from computer-aided design (CAD) analysis. For many spacecraft in LEO, this is the largest disturbance torque.

The second disturbance torque is that of solar radiation pressure (SRP). This is due to absorption and reflection of photons from the Sun. Whether the sunlight is reflected or absorbed will vary with the reflectivity of the surface the light is impinging upon. The SRP will also vary with the attitude of the spacecraft relative to the Sun. This disturbance model, given by Larson [6], is

$$\boldsymbol{L}_{SRP} = \frac{F_S}{c} A(1+r)\cos(\theta)(\boldsymbol{r_{ps}} - \boldsymbol{r_{cm}}), \tag{12}$$

where F_s is the constant solar flux, 1367 W/m^2, c is the speed of light, 3×10^8 m/s, A is a reference surface area, r is the reflectivity of the surface material, conservatively assumed to equal 1, θ is the angle of incidence of the sunlight, $\boldsymbol{r}_{ps}$ is the vector from the satellite origin to the center of solar pressure, and $\boldsymbol{r}_{cm}$ is the vector from the satellite origin to the spacecraft center of mass.

The next disturbance is due to the residual magnetic dipole of the electronics onboard interacting with the Earths magnetic field, and is given by [6]

$$\boldsymbol{L}_{Mag} = \boldsymbol{\mu} \times \boldsymbol{B}, \tag{13}$$

where $\boldsymbol{\mu}$ is the magnetic dipole of the spacecraft and $\boldsymbol{B}$ is the Earth's magnetic field vector. The magnetic dipole is prohibitively difficult to calculate due to the large

amount of circuitry and electronics onboard a satellite, so it is typically measured once a satellite has been fully integrated. For design and simulation purposes, however, it is usually sufficient to assume a value that has been measured by a spacecraft in a similar class. Published data on magnetic dipole measurements can be found in papers by Armstrong et al. [8], Springmann et al. [9], and Inamori et al. [10]. The simulations in the present work are for a cubesat, so the value measured by Armstrong et al., $\mu = 0.009$ *A-m*^{2}, is used. The Earth's magnetic field vector is obtained from a lookup table called the International Geomagnetic Reference Field (IGRF) [11] to produce the true value of $\boldsymbol{B}$.

The final disturbance torque is due to the gravity gradient. This torque is given by [6]

$$\boldsymbol{L}_{GG} = \frac{3\mu_{Earth}}{2R^3}\left|J_z - J_y\right|\sin(2\varphi), \tag{14}$$

where μ_{Earth} is the gravitational parameter of Earth, 3.986×10^{14} m^3/s^2, R is the orbital radius, J_z and J_y are the moments of inertia, and φ is the angle between the z axis and the local horizontal. This disturbance is typically the smallest for cubesat-class missions.

Once all four disturbance torques have been modeled using equations (11)- (14), they are combined for use in equation (8).

$$\boldsymbol{L} = \boldsymbol{L_{Aero}} + \boldsymbol{L_{SRP}} + \boldsymbol{L_{Mag}} + \boldsymbol{L_{GG}} \tag{15}$$

Using a conservative estimate of the maximum disturbance torque magnitude, a conservative estimate of angular acceleration due to disturbance torques can be computed using the spacecraft inertia. This is used in determining the process noise, Q, in the UKF. The details of attitude filter derivation are beyond the scope of this work, and can be found in thorough detail in sources [1], [12], [13], and [14].

With all of the spacecraft dynamics accounted for, sensor measurements are now generated based on the new state.

Sensor Models

Once the state of the satellite has been propagated, sensors are simulated by reading several values and then corrupting them by adding zero-mean Gaussian noise. The sensors used in the simulations consist of a magnetometer, rate gyro, and Sun sensors. Sun sensors have already been described, so modeling the remaining sensors will be described here.

The first sensor, a magnetometer, reads the Earth's magnetic field in the body frame of the satellite, $\boldsymbol{B}$, from the IGRF model and then produces the measured value, $\boldsymbol{B_{meas}}$ from

$$\boldsymbol{B_{meas}} = \boldsymbol{B} + \mathcal{N}(0, \sigma^2)\,, \tag{16}$$

where the notation $\mathcal{N}(\mu, \sigma^2)$ corresponds to a Gaussian random variable with mean μ and standard deviation σ. The noise variance that can be expected from a magnetometer will be found on the hardware datasheet.

The next sensor, rate gyros, have substantially more complex models than magnetometers. This is due to the inherent tendency of gyros to drift over time, which must be accounted for in the model. Rate gyros produce a reading of the spacecraft angular velocity corrupted by both Gaussian noise and a bias error [1], $\boldsymbol{\beta}$, with

$$\boldsymbol{\beta_k} = \boldsymbol{\beta_{k-1}} + \sigma_u \Delta t^{1/2} \mathcal{N}(0, I)\,, \tag{17}$$

$$\boldsymbol{\omega_{meas}} = \boldsymbol{\omega} + \tfrac{1}{2}(\boldsymbol{\beta_k} + \boldsymbol{\beta_{k-1}}) + c_{gyro}\mathcal{N}(0, I)\,, \tag{18}$$

$$c_{gyro} = \left(\frac{\sigma_v{}^2}{\Delta t} + \frac{1}{12}\sigma_u{}^2 \Delta t\right)^{1/2}, \tag{19}$$

where $\boldsymbol{\beta}_k$ is the gyro bias at the current time step in the simulation, $\boldsymbol{\beta}_{k-1}$ is the gyro bias at the previous time step, σ_v is the gyro noise density, and σ_u is the gyro bias noise density. These two noise densities can be either found on hardware datasheets or determined experimentally.

With all of the sensors described, the next subject within numerical methodology is the simulation initialization.

Simulation Initialization

The spacecraft is initialized to a random attitude with an angular velocity of $[0.25, 2.0, 0.25]^T$ deg/s, in sunlight. The attitude estimation system is initialized with the TRIAD algorithm [1] using a measured Sun vector and a magnetometer reading. Since no control torques are active on the system, the spacecraft is free to drift based upon its initial angular velocity and the disturbance torques that act on it.

After the orbital mechanics and rotational dynamics have been propagated at each time step, the sensor readings are generated. Once sensor measurements are available for each sensor, they are passed into an Unscented Kalman Filter [12] [13] algorithm. This algorithm uses the sensor readings, the estimate of the disturbance torque maximum magnitude, and the state estimate at the previous time step to estimate a new dynamic state, consisting of attitude quaternion, angular velocity, and gyro bias.

SIMULATION RESULTS AND DISCUSSION

Error Metrics

At the end of the simulation, the error quaternion is computed at each time step for the output from each of the two filters. This error quaternion is the rotation between the estimated state and the true state. The error

quaternion at each time step is converted to the Euler axis/angle attitude parameterization, not to be confused with Euler angles [15], for further analysis. This requires the use of the small angle approximation, so results with large angles should be carefully scrutinized.

$$\vartheta = 2\,cos^{-1}\left(q_{err,4}\right) \tag{20}$$

The reasoning for this is that although quaternions are highly convenient for computational purposes, it is difficult to interpret their meaning. The Euler axis/angle representation, however, allows an arbitrary rotation to be expressed as a single angle. The axis which this rotation is about will vary and is rarely physically intuitive. However, this is an acceptable tradeoff for the purpose of being able to describe rotational error using a single number.

The errors in roll, ϕ, pitch, θ, and yaw, ψ, are computed from the first three components of the error quaternion [1], and their 3σ bounds are determined from the covariance matrix from the UKF.

$$\phi = 2q_{err,1} \tag{21}$$

$$\theta = 2q_{err,2} \tag{22}$$

$$\psi = 2q_{err,3} \tag{23}$$

The total error in rotational angle is a good first metric to examine when evaluating filter performance. After that, the roll, pitch, yaw, and their 3σ probability bounds provide more detail.

Finally, the number of photodiodes at each time step that have sunlight impinging within their 60° field of view is analyzed as well, to assist with explaining the differences in filter performance.

Results and Discussion

The results of the total rotational angle error are shown in figure 1. Subject to the same initialization and disturbance environment, the filter using the VMM converges much more rapidly to the true attitude than the filter using the SMM does. At only 25 seconds into the simulation, the VMM filter has already converged to within 1° of the true attitude, while the SMM filter takes more than twice as long to get within 4°. The reason for this may be found in figure 2, which shows how many photodiodes are receiving sunlight within their valid field of view. For much of the first 50 seconds, the VMM filter is receiving four, five, or even six photodiode measurements. Meanwhile, the SMM filter is receiving only a single three-dimensional vector reading. Since the VMM filter is receiving more independent readings, it is no surprise that it converges more quickly.

At around 80 seconds into the simulation, the SMM filter experiences a sudden but slight divergence. The attitude estimate jumps from 3° of error up to 6°. The VMM filter also undergoes a small jump in error, but of much smaller magnitude. Once again, the origin of this behavior can be found in figure 2. At this time, the number of valid photodiodes briefly dips down to 2. At this point, the SMM system becomes underdetermined, and cannot compute a vector to the Sun. Thus, the only sensors with any input to the filter are the magnetometer and rate gyro. For the filter running the VMM, however, two photodiode voltages are still able to be read and compared to predictions. While it is not as good as having five or six measurements as was the case earlier in the simulation, it is certainly an improvement over the Sun sensor system being incapable of contributing any information to the attitude estimation system.

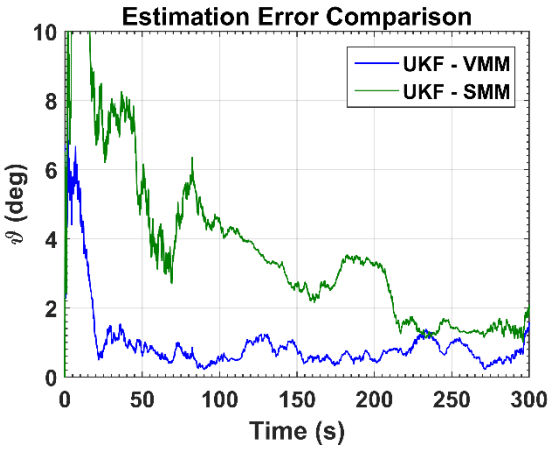

Figure 1: Comparison of estimation system error between the voltage measurement model and Sun measurement model

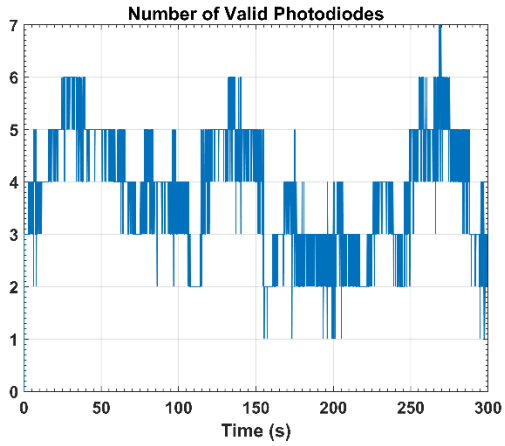

Figure 2: The number of photodiodes at each time step that have light incident upon them at <60 degrees

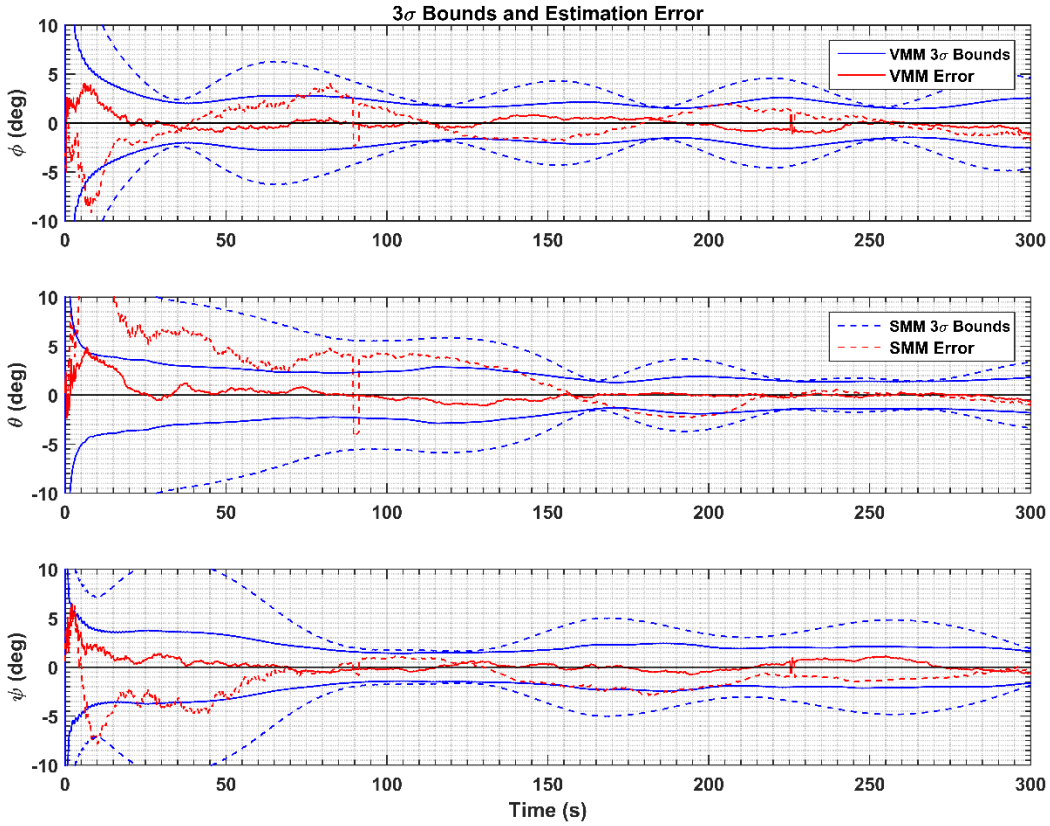

Figure 3: The errors in roll, pitch, and yaw estimation. The 3σ bounds show the confidence of the filter running each measurement model.

The errors in roll, pitch, and yaw, as well as the 3σ probability bounds for them, are shown in figure 3. These errors and bounds support what is shown in figures 1 and 2, that the presence of more sensor readings allows the filter with the VMM model to converge much more quickly. In the time period between 100 and 150 seconds, the SMM filter is gradually converging towards the VMM filter performance which has largely leveled off. This leveling off is due to a combination of sensor noise and disturbance torques. This behavior can be seen in both figures 1 and 3.

Shortly after 150 seconds, the number of available photodiodes once again goes below three, and briefly even reaches one. In this time period between 150 and 200 seconds, the SMM filter can again be observed to suffer performance penalties due to the decreased number of sensor readings. The filter using VMM, however, appears to be more resistant since some photodiodes are still available. When the spacecraft attitude once again allows for enough photodiodes to be read to construct a Sun vector measurement, occurring at about 225 seconds, the SMM filter is able to recover. The two filters have comparable estimate errors for a brief moment at 235 seconds, but then the VMM filter is able to receive more sensor readings starting at 250 seconds. At that point, the VMM filter once again converges to the true state more quickly and the SMM filter is unable to match it again for the rest of the simulation.

CONCLUSIONS

As small satellite missions become more complex, the requirements placed on systems and subsystems grow in difficulty. The ever-expanding market for commercial-off-the-shelf hardware and software is able to alleviate some of the burden that is placed on engineers of small spacecraft, but not all of it. In addition to improvements in hardware and more sophisticated software, algorithms and models must continue to improve as well.

In this work, a new Sun sensor measurement model was proposed for use in attitude estimation systems. Compared to many other algorithms and models that

exist in this field, the new model is not based on some esoteric mathematical derivation, nor on some new physical insight. It is a simple reformulation of the model that already exists, designed with the intent to wring every bit of efficiency possible out of an inexpensive piece of hardware to meet the goal of making cubesat-class missions more capable.

Through the use of high-fidelity simulation, it is shown that the proposed voltage measurement model is able to achieve greater performance than the standard Sun vector measurement model. This is done without any extra cost, computational or otherwise. This gives promise that it may be of value to many small satellite missions as the field continues to grow.

REFERENCES

[1] F. L. Markley and J. L. Crassidis, Fundamentals of Spacecraft Attitude Determination and Control, New York: Springer, 2014.

[2] D. A. Vallado, Fundamentals of Astrodynamics and Applications, Springer Science & Business Media, 2001.

[3] J. C. Springmann and J. W. Cutler, "On-Orbit Calibration of Photodiodes for Attitude Determination," *Journal of Guidance, Control, and Dynamics*, vol. 37, no. 6, pp. 1808-1823, 2014.

[4] R. R. Bate, D. D. Mueller and J. E. White, Fundamentals of Astrodynamics, Courier Corporation, 1971.

[5] H. Schaub and J. L. Junkins, Analytical Mechanics of Space Systems, AIAA, 2003.

[6] W. J. Larson and J. R. Wertz, Space Mission Analysis and Design, Torrance: Microcosm Press, 1992.

[7] NOAA, "US Standard Atmosphere 1976," National Aeronautics and Space Administration, Washington DC, 1976.

[8] J. Armstrong, C. Casey, G. Creamer and G. Dutchover, "Pointing Control for Low Altitude Triple Cubesat Space Darts," in *23rd Annual AIAA/USU Conference on Small Satellites*, Logan, 2009.

[9] J. Springmann, J. Cutler and H. Bahcivan, "Magnetic Sensor Calibration and Residual Dipole Characterization for Application to Nanosatellites," in *AIAA/AAS Astrodynamics Specialist Conference*, Toronto, 2010.

[10] T. Inamori, N. Sako and S. Nakasuka, "Compensation of Time-variable Magnetic Moments for a Precise Attitude Control in Nano- and Micro-satellite Missions," *Advances in Space Research*, vol. 48, no. 3, pp. 432-440, 2011.

[11] S. Macmillan and S. Maus, "International geomagnetic reference field—the tenth generation," *Earth, planets and space*, vol. 57, no. 12, pp. 1135-1140, 2005.

[12] J. L. Crassidis and F. L. Markley, "Unscented filtering for spacecraft attitude estimation," *Journal of guidance, control, and dynamics*, pp. 536-542, 2003.

[13] J. L. Crassidis and J. L. Junkins, Optimal Estimation of Dynamic Systems, CRC Press, 2011.

[14] J. L. Crassidis, F. L. Markley and Y. Chen, "Survey of Nonlinear Attitude Estimation Methods," *Journal of Guidance, Control, and Dynamics*, vol. 30, no. 1, pp. 12-28, 2007.

[15] M. Shuster, "A Survey of Attitude Representations," *Journal of the Astronautical Sciences*, vol. 41, no. 4, pp. 439-517, 1993.